WILEY

RESEARCH ARTICLE

Novel noninvasive identification of patient-specific epileptic networks in focal epilepsies: Linking single-photon emission computed tomography perfusion during seizures with resting-state magnetoencephalography dynamics

Balu Krishnan[1] (iD) | Simon Tousseyn[2] | Zhong Irene Wang[1] | Hiroatsu Murakami[1] |
Guiyun Wu[1] | Richard Burgess[1] | Leonidas Iasemidis[3,4] | Imad Najm[1] |
Andreas V. Alexopoulos[1]

[1]Neurological Institute, Epilepsy Center, Cleveland Clinic, Cleveland, Ohio, USA

[2]Academic Center for Epileptology, Kempenhaeghe and Maastricht UMC+, Heeze, The Netherlands

[3]Department of Translational Neuroscience, Barrow Neurological Institute, Scottsdale, Arizona, USA

[4]Department of Neurology, Barrow Neurological Institute, Scottsdale, Arizona, USA

Correspondence
Balu Krishnan, 9500 Euclid Ave, S51, Epilepsy Center, Cleveland, OH 44195, USA.
Email: krishnb@ccf.org

Abstract

Single-photon emission computed tomography (SPECT) during seizures and magnetoencephalography (MEG) during the interictal state are noninvasive modalities employed in the localization of the epileptogenic zone in patients with drug-resistant focal epilepsy (DRFE). The present study aims to investigate whether there exists a preferentially high MEG functional connectivity (FC) among those regions of the brain that exhibit hyperperfusion or hypoperfusion during seizures. We studied MEG and SPECT data in 30 consecutive DRFE patients who had resective epilepsy surgery. We parcellated each ictal perfusion map into 200 regions of interest (ROIs) and generated ROI time series using source modeling of MEG data. FC between ROIs was quantified using coherence and phase-locking value. We defined a generalized linear model to relate the connectivity of each ROI, ictal perfusion z score, and distance between ROIs. We compared the coefficients relating perfusion z score to FC of each ROI and estimated the connectivity within and between resected and unresected ROIs. We found that perfusion z scores were strongly correlated with the FC of hyper-, and separately, hypoperfused ROIs across patients. High interictal connectivity was observed between hyperperfused brain regions inside and outside the resected area. High connectivity was also observed between regions of ictal hypoperfusion. Importantly, the ictally hypoperfused regions had a low interictal connectivity to regions that became hyperperfused during seizures. We conclude that brain regions exhibiting hyperperfusion during seizures highlight a preferentially connected interictal network, whereas regions of ictal hypoperfusion highlight a separate, discrete and interconnected, interictal network.

Abbreviations: BOLD, blood oxygenation level dependent; DRFE, drug-resistant focal epilepsy; EZ, epileptogenic zone; FC, functional connectivity; MEG, magnetoencephalography; PET, Positron emission tomography; PLV, phase-locking value; ROI, region of interest; SEEG, stereo-electroencephalography; SPECT, single-photon emission computed tomography; SISCOM, subtraction ictal SPECT co-registered to MRI.

1 | INTRODUCTION

Growing evidence characterizes epilepsy as a disorder of brain networks involving regions extending well beyond the epileptogenic zone (EZ) (Kramer & Cash, 2012). The epileptic network constitutes structurally and functionally connected brain regions that explain the complex seizure dynamics and are essential for ictogenesis and maintenance of the epileptic condition (Spencer, 2002). Understanding the properties of the epileptic network directly contributes to more accurate localization of the EZ and advances the management of patients with drug-resistant focal epilepsy (DRFE) including placement of intracranial electrodes and individualization of closed-loop neuromodulation approaches for seizure control.

Advances in noninvasive imaging technologies such as magnetic resonance imaging (MRI), positron emission tomography (PET), subtraction ictal SPECT co-registered to MRI (SISCOM), coupled with the measurement of electrophysiological activities via scalp electroencephalography (EEG), magnetoencephalography (MEG), and invasive EEG (e.g., stereo-EEG/SEEG recordings with stereotactically placed depth electrodes) in the same patients, provide us with unique clinical opportunities to understand normal and abnormal activities of neuronal ensembles and their interactions between and during seizures. Moreover, the integration of information from various imaging and nonimaging modalities is fundamental to the generation of clinical hypotheses in the modern management of patients with DRFE (Knowlton et al., 2008). Multimodal integration allows access to complementary information and improves the understanding of the clinical presentation of an individual's neurological disorder.

Ictal SPECT utilizes isotope injection *during seizures* to noninvasively approximate the EZ in patients with DRFE undergoing presurgical evaluation (Kaminska et al., 2003; Newton et al., 1995). The complex hyperperfusion patterns unique to ictal SPECT reflect seizure onset and propagation pathways (Cleeren et al., 2016; Van Paesschen, 2004). We have previously shown that SPECT-directed SEEG planning allows for a more complete electrographic sampling of salient areas, which in turn correlate with specific SEEG electrophysiological signals (power "fingerprints") in the course of SEEG-recorded seizures (Englot & Lagrange, 2022; Krishnan et al., 2021).

MEG relies on *interictal* recordings of spontaneously occurring epileptiform activities to noninvasively approximate the EZ in these patients (Murakami et al., 2016). MEG offers a direct measurement of whole-brain neuronal activity while preserving high spatial and temporal resolution. Traditionally, MEG-based EZ localization relies on source modeling of interictal epileptiform abnormalities. The role of functional connectivity (FC) analysis of MEG data for localization of the EZ has been gaining prominence recently (Krishnan et al., 2015). Integration of information from SPECT and MEG aids in the noninvasive presurgical evaluation of patients with DRFE (El Tahry et al., 2018; Schneider et al., 2013).

Intracranial studies have coarse spatial sampling limited by clinical considerations and ill-posed hypotheses. Sampling using intracranial electrodes is more likely to include areas of SPECT hyperperfusion (that corresponds to the presumed seizure onset and propagation pathways) rather than areas of ictal hypoperfusion (that do not provide clear localizing information). MEG provides a global view of electrophysiological brain dynamics. Using MEG-based source modeling analysis, we can investigate whole-brain cortical activity in the interictal state. Such analysis cannot be realistically achieved with the limited sampling of brain areas that are investigated with implanted electrode recordings.

In this study, we layout a framework for integrating information acquired from ictal SPECT and interictal MEG and thereby characterize the resting-state FC within the ictally hyperperfused and hypoperfused brain regions in a consecutive series of patients who underwent presurgical evaluation at our center. We hypothesize that there is a preferential FC during rest within regions that show significant hyperperfusion or hypoperfusion during seizures. To test this hypothesis, we informed our resting MEG FC analysis by the results of SPECT perfusion patterns during seizures. This allows for an estimation of FC that is driven by measurable nodes of patient-specific epileptic networks, substantiated by our previous studies, which examined the relationships of ictal SPECT perfusion patterns to both evoked and spontaneous SEEG recordings (Krishnan et al., 2021; Tousseyn et al., 2017).

2 | MATERIALS AND METHODS

2.1 | Inclusion and exclusion criteria

The retrospective study was approved by the Cleveland Clinic Institutional Review Board. We included a consecutive series of patients with DRFE who: (1) underwent an interictal MEG and an ictal SPECT as part of their noninvasive presurgical evaluation, (2) had a subsequent SEEG evaluation between January 2015 and December 2016, and finally (3) underwent surgical resection, and (4) had a good quality postoperative MRI. Patients were excluded from the analysis: (1) if SPECT injection had been obtained during the postictal rather than the ictal phase and (2) if brain surgery had been performed between the SPECT/MEG and SEEG evaluations.

2.1.1 | SPECT acquisition and processing

Techniques used for the acquisition and processing of SPECT in this study have been described elsewhere (Tousseyn et al., 2017) and are also provided in supplementary materials S1.

2.1.2 | MEG data acquisition and modeling

MEG data for this study were derived from 1-h clinical recording obtained with a 306-channel whole-head MEG system (Elekta, Sweden) with a sampling rate of 1000 Hz, and application of a band-pass acquisition filter with cut-off frequencies of 0.1 and 333 Hz. MEG data were postprocessed using temporally extended signal space separation (tSSS) algorithm (Taulu & Hari, 2009), which compensates for the magnetic interference caused by external and nearby sources and minor head movements in the MEG array (Kakisaka et al., 2012).

2.1.3 | MEG and MRI preprocessing

Figure 1 describes the analysis pipeline used for the integration of SPECT and MEG data. For FC analysis, we bandpass filtered the tSSS-processed MEG data using a Kaiser filter with passband edges at 1 and 70 Hz and downsampled the data to 200 Hz for computational efficiency using the freely available *Matlab* toolbox *Brainstorm* (Tadel et al., 2011). We identified 5 min of artifact-free data. No constraints regarding the state of the brain, and the presence, or absence of interictal epileptiform discharges were laid during data selection. We downloaded the preoperative MRI DICOM (Digital Imaging and Communications in Medicine) images and performed cortical reconstruction using *Freesurfer* (Dale et al., 1999). The reconstructed surfaces, MRI, and MEG data were imported to *Brainstorm*. The MEG sensors and cortical surfaces were co-registered using the digitized head points (approximately 100 points) collected during MEG acquisition. We constructed the forward model using the overlapping sphere model (Huang

et al., 1999) and used dynamical statistical parametric mapping (dSPM) (Dale et al., 2000) estimates to create the inverse model.

2.1.4 | Estimation of connectivity measures

We constructed a total of 200 regions of interest (ROIs) for MEG FC analysis by parcellating the SISCOM perfusion pattern using k-means clustering (Figure 2a,b, See Supplementary material S1). The parcellated map was imported into *Brainstorm* as a volume atlas and converted to "scouts." Each scout served as ROI for our analysis. The average ROI area across patients was found to be 11 cm^2 ($\sigma = 4$ cm^2). We estimated the average SISCOM perfusion z score (Z_i) for every ROI. We used inverse modeling to estimate the source time series. We then averaged all the sources within an ROI to generate a single time series per ROI. We expected some of the sources within an ROI to have opposite orientations. To offset this, we flipped the sign of sources with opposite orientations before averaging. Finally, we performed independent component analysis (ICA) based decomposition of the ROI time series to remove any residual EKG artifacts that were not removed during tSSS processing (Hyvärinen & Oja, 2000). For every 5-s segment of the ROI time series (derived from the 5-min period of MEG data in each patient), we estimated coherence (COH) (Bokil et al., 2010; Thomson, 1982) and phase-locking value (PLV) (Lachaux et al., 1999) between brain regions for the delta (0–4 Hz), theta (4–8 Hz), alpha (8–12 Hz), beta (12–30 Hz), and gamma (30–70 Hz) frequency bands (see Supplementary material S2). Connectivity measures were averaged across the 60 segments and used in the subsequent analysis.
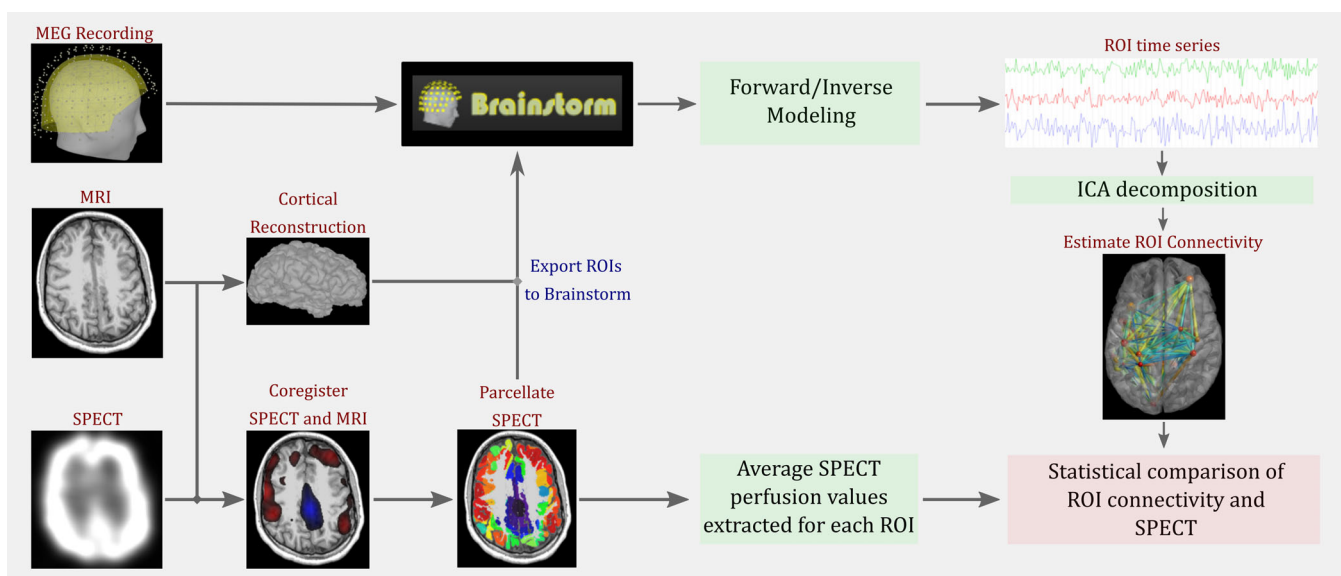
FIGURE 1 Pipeline used for comparing ictal single-photon emission computed tomography (SPECT) and magnetoencephalography (MEG) functional connectivity. We first perform cortical reconstruction of the patient's magnetic resonance imaging (MRI) using *Freesurfer*. We then co-register the ictal SPECT data to the MRI and parcellate the resulting SPECT data. Next, we import the temporally extended signal space separation (tSSS)-processed MEG time series, the reconstructed cortical surfaces, and the regions of interest (ROIs) generated from SPECT data to *Brainstorm*. We perform source modeling analysis of the MEG data and generate a time series per ROI. We then use ICA decomposition to remove any residual EKG artifacts that were not rejected during tSSS processing. Next, we perform connectivity analysis of the resulting time series using coherence and phase locking value. Finally, we perform statistical analysis of the ROI connectivity and SPECT perfusion values.
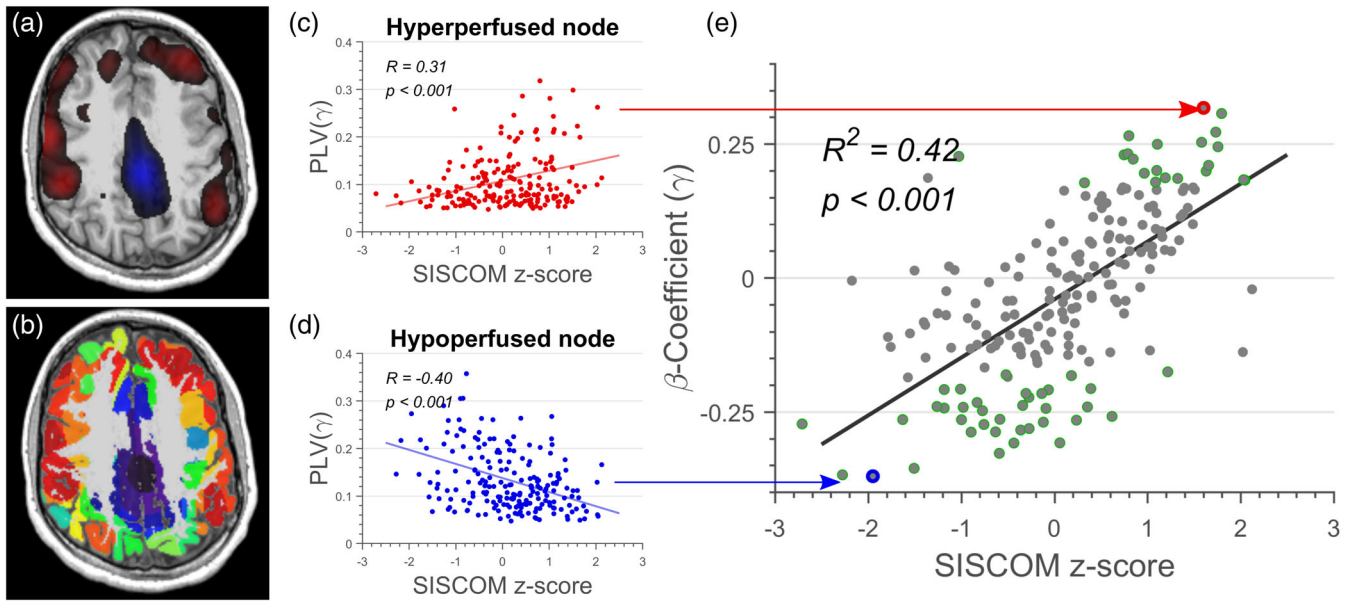
FIGURE 2 (a) Ictal single-photon emission computed tomography (SPECT) pattern of hyperperfusion (red blobs) and hypoperfusion (blue blobs) for Patient P05. (b) Parcellation of the cortical surface using subtraction ictal SPECT co-registered to MRI (SISCOM) z value. (c, d) Relationship between SISCOM perfusion z value and phase-locking value for: (c) a hyperperfused node and (d) a hypoperfused node. (e) Relationship between SISCOM z value and β_1-coefficient for Patient P05. Each grey shaded circle represents 1 out of 200 regions of interest (ROIs). ROIs with statistically significant β_1-coefficients are denoted using green borders.

2.1.5 | Definition of SPECT hyperperfusion and hypoperfusion

Newey et al. defined the optimal SISCOM z-threshold for identifying the EZ as 1.5, which corresponds to a p value of .07 (Newey et al., 2013). In line with this finding, we defined hyperperfused and hypoperfused brain regions as the ROIs with the top and bottom 7% SISCOM z scores, respectively. ROIs that were not identified as hyperperfused or hypoperfused were categorized as regions of baseline perfusion (i.e., ROIs that had no significant change in perfusion during the seizure).

2.1.6 | Correlating SPECT perfusion and resting-state connectivity

Based on our previous work (Tousseyn et al., 2017), we hypothesized that hyperperfused ROIs will be strongly connected to other hyperperfused ROIs, whereas hypoperfused ROIs will be strongly connected to other hypoperfused ROIs. To identify ROIs with high correlation with SISCOM z score, the distribution of the connectivity profile of an ROI was compared to SISCOM z score. To be unbiased in our approach, this relationship was evaluated for all ROIs in the same patient. The following regression model was constructed to evaluate the relationship between perfusion map and connectivity (Figure 2c,d). For every ROI i, we estimate the beta coefficients ($\beta_{0,f}^i, \beta_{1,f}^i, \beta_{2,f}^i$) such that

$$C_f^{ji} = \beta_{0,f}^i + \beta_{1,f}^i Z^j + \beta_{2,f}^i d^{ji} \quad \forall j \neq i \quad (1)$$

where C_f^{ji} is the connectivity estimated using coherence or PLV between nodes i and j for frequency band f. Z^j is the SISCOM z score of node j and d^{ji} is the Euclidean distance between the nodes i and j. The distance variable was included in the regression model to remove any distance-modulated variance from the β_1 estimates (Honey et al., 2009). Thus, the β_1 estimates for ROI i relate the FC of ROI i to the SISCOM perfusion z score. We then generate β_1 estimates for every ROI and for the five frequency bands in each individual patient. Since this results in a large number of statistical comparisons, we used the methods described in Benjamini and Hochberg to adjust the p values associated with the β_1 estimates (Benjamini & Hochberg, 1995).

A positive and statistically significant β_1 estimate for ROI i indicates that FC estimates of ROI i and SISCOM perfusion z score have similar covariance. We used cross-correlation analysis to evaluate the relationship between β_1^i estimates, and the SISCOM perfusion z score (Z^i) of ROI i to test whether regions with higher perfusion z score have higher β_1 estimates while those with lower perfusion z score have lower β_1 estimates in every single patient (Figure 2e). Finally, the distribution of statistically significant β_1 estimates were compared for ROIs identified as hyper-, hypo-, and baseline perfused to check whether hyperperfused ROIs have a higher fraction of positive β_1 estimates and hypoperfused ROIs have a higher fraction of negative β_1 estimates.

2.1.7 | Connectivity between the area of surgical resection and perfusion pattern

The postoperative MRI was co-registered to the patient's preoperative MRI and the region of surgical resection was hand-drawn. We
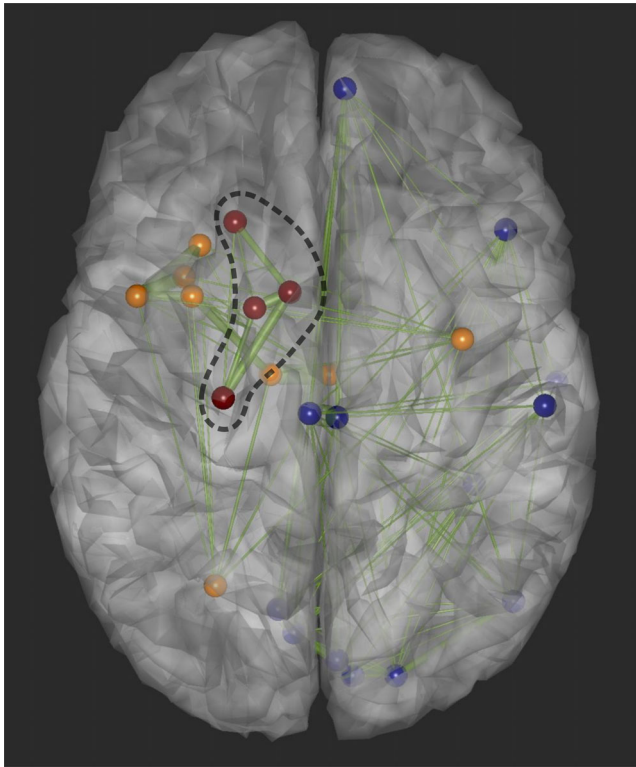
FIGURE 3 Schematic visualization of the hyperperfused regions of interest (ROIs) that were resected (in red), hyperperfused ROIs that were not resected (in orange), and hypoperfused ROIs (in blue). The dashed black curve denotes the surgical resection margin.

identified the ROIs that were part of the surgical resection, which helped us divide the brain regions into four zones: hyperperfused ROIs inside (Z_{R+}^+) and outside (Z_{R-}^+) the area of surgical resection, ROIs with baseline perfusion outside (Z_{R-}^0), and hypoperfused ROIs outside (Z_{R-}^-) the area of surgical resection. A schematic visualization of the zones is shown in Figure 3. We were then able to investigate the connectivity linking perfusion with the area of surgical resection. Specifically, we estimated and statistically compared the average intrinsic (within-group) connectivity: Z_{R+}^+, Z_{R-}^+, Z_{R-}^0, Z_{R-}^-, and the average extrinsic (between-group) connectivity: $Z_{R+}^+ - Z_{R-}^+$, $Z_{R+}^+ - Z_{R-}^0$, $Z_{R+}^+ - Z_{R-}^-$, $Z_{R-}^+ - Z_{R-}^-$, $Z_{R-}^+ - Z_{R-}^0$, and $Z_{R-}^- - Z_{R-}^0$. For intrinsic connectivity analysis, we only analyzed patients who had at least two ROIs within each group.

2.1.8 | Subgroup analysis

We performed subgroup analysis to compare the correlation between SISCOM z scores and β_1-coefficients in the following conditions: (1) seizure-free versus nonseizure-free outcome, (2) early versus late ictal SPECT injection, (3) secondarily generalized (focal to bilateral tonic–clonic) seizure versus nongeneralized SPECT seizure, and (4) unifocal versus multifocal epilepsy. We also compared the average

connectivity within hyperperfused and hypoperfused ROIs between patients who were in a state of wakefulness and sleep during the MEG study.

2.1.9 | Statistical considerations

We used the Students' t test to assess the statistical significance of population-level correlation coefficients and the Shapiro–Wilke test to examine the normality of the distribution. We compared the differences in intrinsic and extrinsic connectivity within and between the four groups: Z_{R+}^+, Z_{R-}^+, Z_{R-}^0, Z_{R-}^- with paired Mann–Whitney U-test. Further, we employed analysis of variance (ANOVA) to assess the influence of timing of ictal SPECT injection, seizure duration, and resective surgery outcome on intrinsic and extrinsic connectivity. We defined early ictal SPECT injections as SPECT studies with injection time that was shorter or equal to the median injection time across the 30 patients included in the study. Similarly, we defined short-duration seizures as ictal SPECT seizures, which had a duration that was shorter than or equal to the median seizure duration across all patients. We used the methods described by Benjamini and Hochlberg to adjust for multiple comparisons and control the type I error rate (Benjamini & Hochberg, 1995).

3 | RESULTS

3.1 | Study population

Out of all patients who had ictal SPECT, SEEG, and MEG for localization of the EZ between January 2015 and December 2016, 30 patients met the specific inclusion criteria (see Table 1). No patient had prior resective epilepsy surgery. The median age of the study population was 27.5 years (range: 8–58 years), and the male: female ratio was 18:12. The median age at seizure onset was 15 years (range: 0–46 years) and the median duration of epilepsy was 10.5 years (range: 2–36 years). The median SPECT injection time was 18 s (range: 1–220 s) with a median seizure duration of 83.5 s (range: 16–390 s). Fifteen patients were seizure-free after resective surgery. The median postoperative follow-up period was 23 months (range: 6–40 months). Thirteen patients had more than one area of SEEG onset. These patients demonstrated nonadjacent areas of SEEG onset and were therefore deemed as "multifocal."

3.1.1 | Comparison between unthresholded SISCOM z score and resting-state connectivity

Figure 2 shows representative results in a single patient. Figure 2c,d shows the gamma band FC estimated using PLV, as a function of

TABLE 1 Patient demographics

Patient ID	Age	Age at epilepsy onset	SICOM details (s) Injection time	Flush time	Seizure duration	MRI	ILAE outcome (follow-up time, months)	Pathology
P01	19	10	12	17	73	Increased FLAIR signal in bilateral hippocampal formation (L > R)	I (35)	FCD
P02	29	23	18	21	97	Nonlesional	I (25)	FCD
P03	27	17	4	11	280	Nonlesional	V (21)	FCD/nodular heterotopia
P04	26	6	11	16	66	Nonlesional	V (23)	FCD
P05	15	8	16	25	139	Mildly asymmetrical increase in FLAIR signal within right hippocampus, parahippocampal gyrus and amygdala	I (20)	FCD
P06	32	18	20	23	103	Nonlesional	I (40)	FCD
P07	8	6	20	22	141	Left temporal hyperintensity	I (9)	FCD
P08	42	17	12	16	68	Nonlesional	IV (18)	FCD
P09	25	21	23	28	113	Extensive periventricular nodule heterotopias	III (9)	FCD
P10	27	2	45	49	74	Subtle increased signal in R. occipital/posterior temporal regions involving cortex and subcortical regions	I (12)	FCD
P11	28	20	15	19	75	Nonlesional	I (11)	Gliosis
P12	34	30	4	9	70	Nonlesional	III (13)	Gliosis
P13	32	25	21	23	390	Mild left hippocampal atrophy	I (12)	Gliosis
P14	56	20	10	13	34	Non-lesional	I (12)	Not available
P15	29	7	18	22	79	Right. Intraventricular mass (caudate)	V (13)	Gliosis
P16	35	13	22	24	59	Nonlesional	I (32)	Gliosis
P17	18	16	22	26	84	Slight decrease in size of left hippocampus	I (6)	FCD
P18	58	46	23	24	134	Nonlesional	IV (25)	FCD
P19	30	22	11	15	95	Heterotopic gray matter along margins of lateral ventricles	IV (25)	Gliosis
P20	35	0	19	23	90	Symmetrical volume loss in parieto-occipital lobes/superior and middle frontal gyri	IV (29)	Gliosis
P21	25	6	220	224	256	Nonlesional	IV (34)	Gliosis
P22	19	8	8	12	16	Decreased size in bilateral hippocampi, blurring of mesial aspects of R. superior frontal gyrus	I (13)	FCD
P23	25	5	5	10	118	Nonlesional	V (34)	FCD
P24	40	35	51	55	149	Nonlesional	I (33)	Gliosis
P25	26	20	17	21	75	Nonlesional	I (36)	FCD
P26	43	35	17	20	20	Mild and symmetric volume loss in bilateral hippocampal	IV (17)	Gliosis
P27	26	1	7	17	70	Nonlesional	IV (23)	FCD
P28	21	14	26	31	83	Nonlesional	IV (24)	Not available
P29	31	0	23	27	105	Subtle increased signal in the right amygdala/hippocampal	I (25)	Gliosis
P30	26	10	20	22	19	Nonlesional	IV (40)	FCD

Abbreviations: FCD, focal cortical dysplasia; MRI, magnetic resonance imaging; SISCOM, subtraction ictal SPECT co-registered to MRI.

SISCOM z score for a hyperperfused and hypoperfused node, respectively. We observed a statistically significant ($p < .001$) and positive correlation ($R^2 = .42$) between SISCOM z scores in each node and the corresponding β_1-coefficients (Figure 2e).

Distribution of correlation coefficient between SISCOM z scores and β_1-coefficient across patients estimated using PLV and coherence is shown in Figure 4a,b, respectively. We observed a statistically significant ($p < .001$) and positive correlation between SISCOM z scores and β_1-coefficients across frequency bands. A higher correlation was observed when using PLV as a connectivity measure, as compared to coherence analysis.

We also evaluated the statistical significance of the correlation between SISCOM z scores and β_1-coefficients for individual patients. All patients had a statistically significant ($p < .001$) and positive correlation when PLV was used as the connectivity measure. For coherence-based FC analysis, a statistically significant ($p < .05$) and positive correlation was observed across frequency bands for 77%–80% of the patients. No correlation between β_1-coefficient and SISCOM z scores was appreciated in the remaining 20%–23% of patients.

### 3.1.2 | Comparison between thresholded SISCOM z scores and resting-state connectivity

Figure 5 shows the distribution of β_1-coefficients estimated using PLV in the three ROI groups: hypo-, baseline- and hyper-perfused. Among the hypoperfused ROIs, a statistically significant ($p < .003$) higher fraction of ROIs have negative—compared to positive—significant β_1-coefficients (Figure 5a). The hyperperfused ROIs tend to have a statistically significant ($p < .001$) higher fraction of positive—compared to negative—significant β_1-coefficients (Figure 5c). For baseline-perfused regions, there was no statistically significant difference ($p > .17$) between the fraction of ROIs with positive versus negative significant β_1-coefficients (Figure 5b). Results were similar when using coherence as connectivity estimator (Figure S2).

3.1.3 | Subgroup analysis

We did not find any statistically significant difference among our four subgroups when examining the correlation between SISCOM z scores
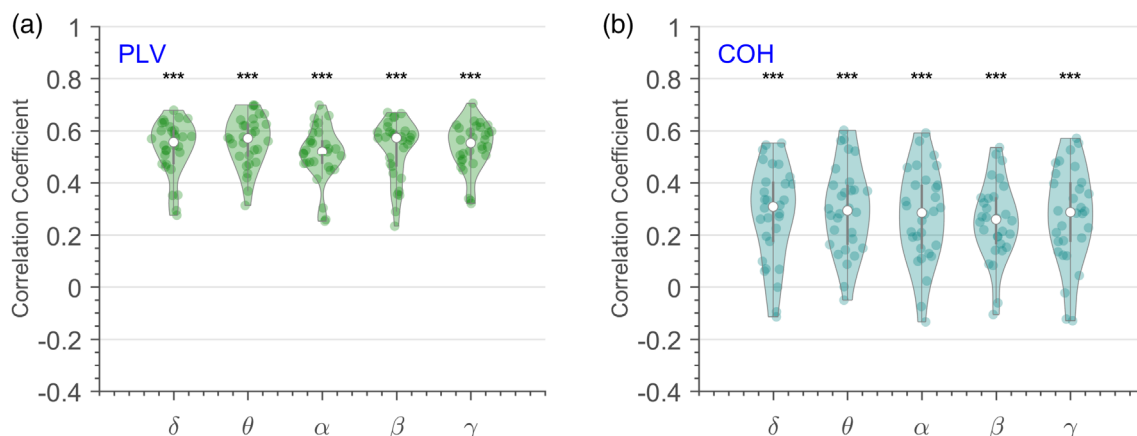
FIGURE 4 Distribution of the cross-correlation coefficient between β_1-coefficients and subtraction ictal SPECT co-registered to MRI (SISCOM) z values across patients and frequency bands when estimating connectivity using (a) phase-locking value, and (b) coherence. Asterisks denote statistically significant ($p < .001$) and positive correlation between β_1 distribution and SISCOM z score across patients.
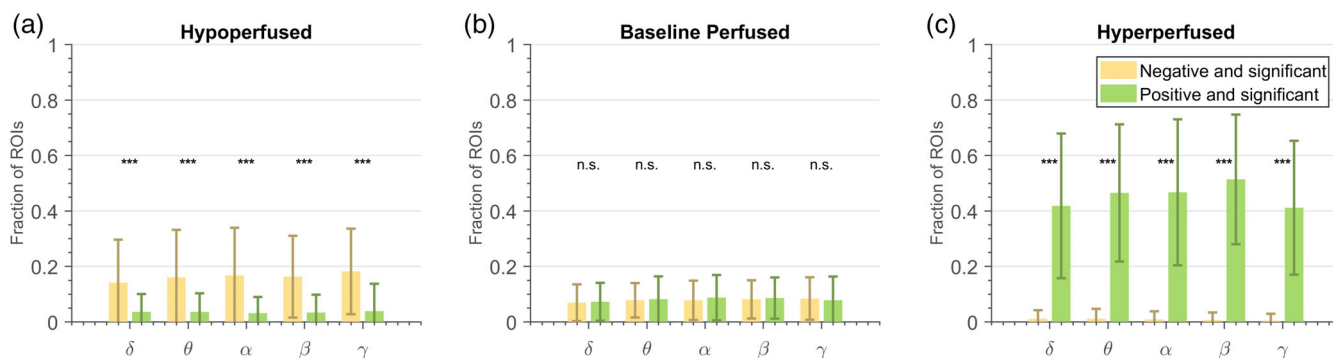
FIGURE 5 Distribution of β_1-coefficients for the (a) hypoperfused regions of interest (ROIs), (b) baseline perfused ROIs—that is, ROIs that showed no significant change in perfusion during the seizure, and (c) hyperperfused ROIs. Single ($p < .05$), double ($p < .01$) or triple ($p < .001$) asterisks denote a statistically significant difference between the fractions of ROIs that have negative versus positive β_1-coefficients. Phase-locking value (PLV) was used as the connectivity estimator.

and β_1-coefficients across all frequency bands: (1) seizure-free versus nonseizure-free outcome ($p > .32$), (2) early versus late ictal SPECT injection ($p > .10$), (3) secondarily generalized versus nongeneralized SPECT seizure ($p > .66$), (4) uni-focal versus multifocal epilepsy ($p > .88$). The differences were not significant irrespective of the method used to estimate FC.

3.1.4 | Difference in connectivity between patients in state of wakefulness and sleep

We identified 6 patients to be in a state of wakefulness, 20 patients in sleep, and 4 patients to be partly awake and then asleep in 5 min of MEG data used for connectivity analysis. We observed a statistically significant ($p < .023$) and higher FC in the alpha frequency band within regions of hypoperfusion in those patients who were in a state of wakefulness, when compared to patients who were asleep. These findings were statistically significant only when PLV was used as connectivity estimator.

3.1.5 | Connectivity between perfusion inside and outside area of surgical resection

Intrinsic connectivity
Using PLV-based connectivity estimates, the highest intrinsic connectivity across all patients ($p < .0012$; Figure 6) was observed for regions that showed hyperperfusion inside ($Z_{R_+}^+$) and outside ($Z_{R_-}^+$) the resection cavity, when compared to nonresected baseline-perfused ($Z_{R_-}^0$), and hypoperfused ($Z_{R_-}^-$) regions. Even though resected areas of hyperperfusion had higher connectivity when compared to nonresected areas of hyperperfusion, these differences were not statistically significant ($p > .13$). Finally, we observed a higher and statistically significant connectivity ($p < .009$) within hypoperfused and nonresected ($Z_{R_-}^-$) regions, as compared to baseline-perfused and nonresected ($Z_{R_-}^0$) ROIs. These results were largely consistent across frequency bands, measures used to estimate connectivity, and distance between ROIs (Figure S3).

When using coherence as a connectivity estimator, we observed a higher and statistically significant intrinsic connectivity within ROIs inside the resection ($Z_{R_+}^+$), when compared to those outside the area of resection ($Z_{R_-}^+$) (Figure 7).

Extrinsic connectivity
A statistically significant and higher connectivity between hyperperfusion inside and outside the area of resection ($Z_{R_+}^+ - Z_{R_-}^+$), as compared to other extrinsic groups ($p < .001$; Figure 6, 7), was apparent irrespective of frequency bands and measures used to estimate connectivity.

Effect of surgical outcome, ictal SPECT injection time, and seizure duration
Neither the intrinsic nor the extrinsic connectivity was statistically different between seizure-free and nonseizure-free patients, early versus late ictal SPECT injection, and short versus long seizure duration.

When using coherence as intrinsic FC estimator, we found that the difference between ROIs inside ($Z_{R_+}^+$) versus outside ($Z_{R_-}^+$), the resection cavity, was statistically significant only in the seizure-free patients ($p < .006$). The difference was not significant in the nonseizure-free group ($p > .26$). While we observed higher connectivity within regions included within the resection ($Z_{R_+}^+$) regions compared to those outside ($Z_{R_-}^+$), the differences were not significant, when using PLV as connectivity estimator. For the seizure-free group, 11 patients had at least two or more nodes that were hyperperfused and resected. For the nonseizure-free group, six patients had at least two or more nodes that were hyperperfused and resected.

4 | DISCUSSION

MEG and SPECT are complementary but invaluable tools for the non-invasive localization of the EZ. Interpretation of the complex perfusion patterns observed in ictal SPECT studies is often challenging (Dupont et al., 2006). The areas of hyperperfusion reflect the ictal onset and propagation pathways and thus represent measurable nodes of an interconnected seizure-related network (Krishnan et al., 2021; Van Paesschen, 2004). The present study aims to promote the clinical understanding and interpretation of these complex perfusion patterns by incorporating resting-state FC analysis.

4.1 | Main findings

4.1.1 | Subtraction ictal SPECT

We found the existence of a very strong correlation between SISCOM perfusion z scores and FC estimates within hyperperfused and hypoperfused ROIs. These findings suggest that hyperperfused brain regions are preferentially connected to other areas of hyperperfusion, and by the same token ictally hypoperfused brain regions are preferentially connected to other areas of hypoperfusion. Thus, human seizures invoke neuronal pathways that are active even during rest. One explanation would be that epileptogenic networks are embedded in preformed physiological and/or individualized brain networks (Halász, 2010). Whole-brain perfusion changes during seizures are bound to be complex but also contain rich information regarding preferential and patient-specific brain connectivity. In clinical practice, ictal SPECT analysis is sometimes watered down to a mere (and often insufficient) tool for seizure localization. Our study should prompt us to view and interpret seizure related (increases and decreases) in SPECT perfusion patterns with a brain network perspective in our mind.

4.1.2 | Electrophysiological connectivity in hyperperfusion and hypoperfusion

Hyperperfusion
We found a positive and statistically significant β_1-coefficients across all patients in regions that show hyperperfusion during seizures. The

FIGURE 6 Distribution of phase-locking value (PLV)-based intrinsic and extrinsic connectivity for the five frequency bands across all patients. Statistically significant differences between connectivity estimates are denoted with single ($p < .05$), double ($p < .01$), and triple ($p < .001$) asterisks.

Z_{R+}^{+}: hyperperfused nodes inside resection

Z_{R-}^{0}: baseline perfused nodes outside resection

Z_{R-}^{+}: hyperperfused nodes outside resection

Z_{R-}^{-}: hypoperfused nodes outside resection

FIGURE 7 Distribution of coherence-based intrinsic and extrinsic connectivity for the five frequency bands across all patients. Statistically significant differences between connectivity estimates are denoted with single ($p < .05$), double ($p < .01$), and triple ($p < .001$) asterisks.
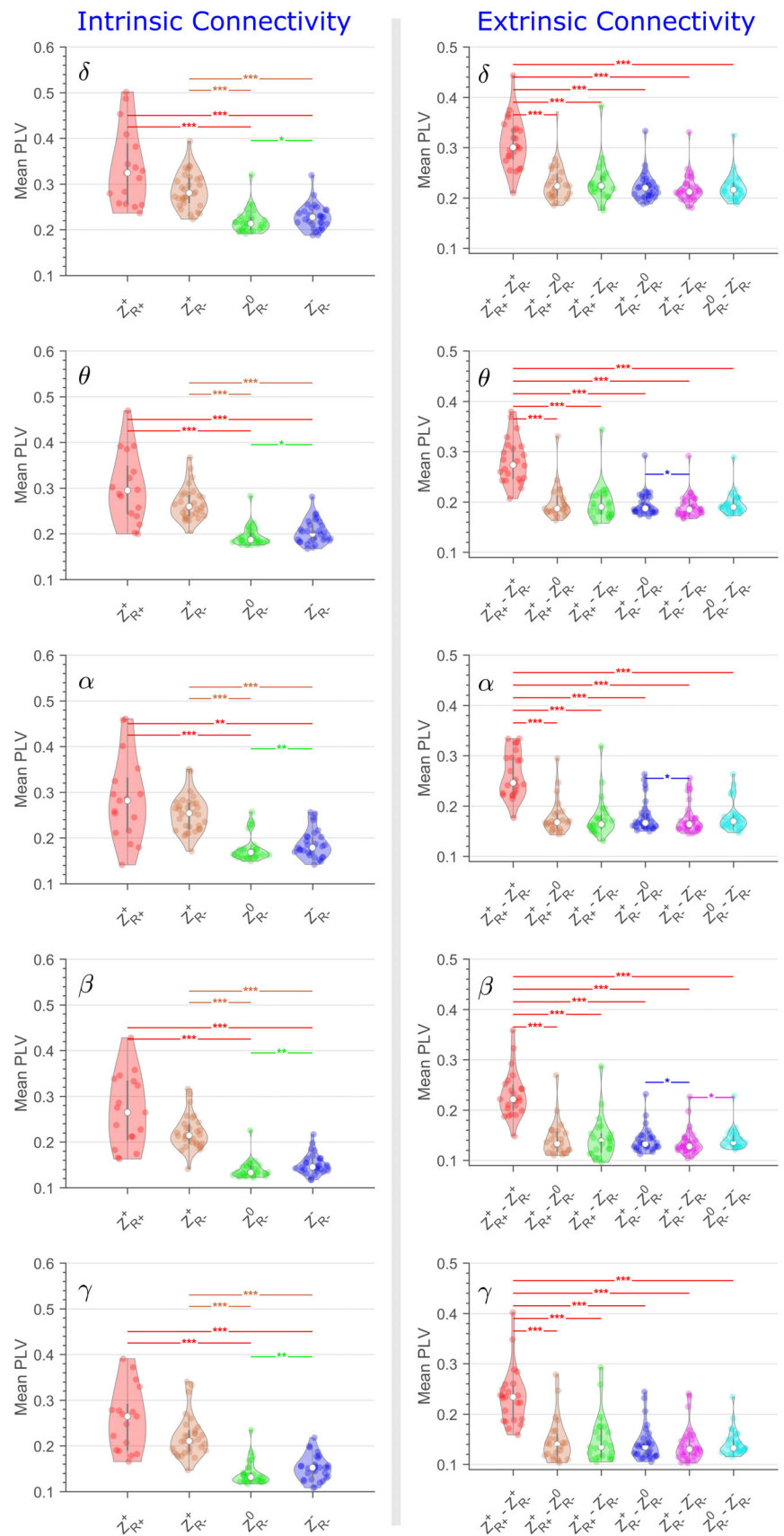
Z_{R+}^+: hyperperfused nodes inside resection

Z_{R-}^+: hyperperfused nodes outside resection

Z_{R-}^0: baseline perfused nodes outside resection

Z_{R-}^-: hypoperfused nodes outside resection
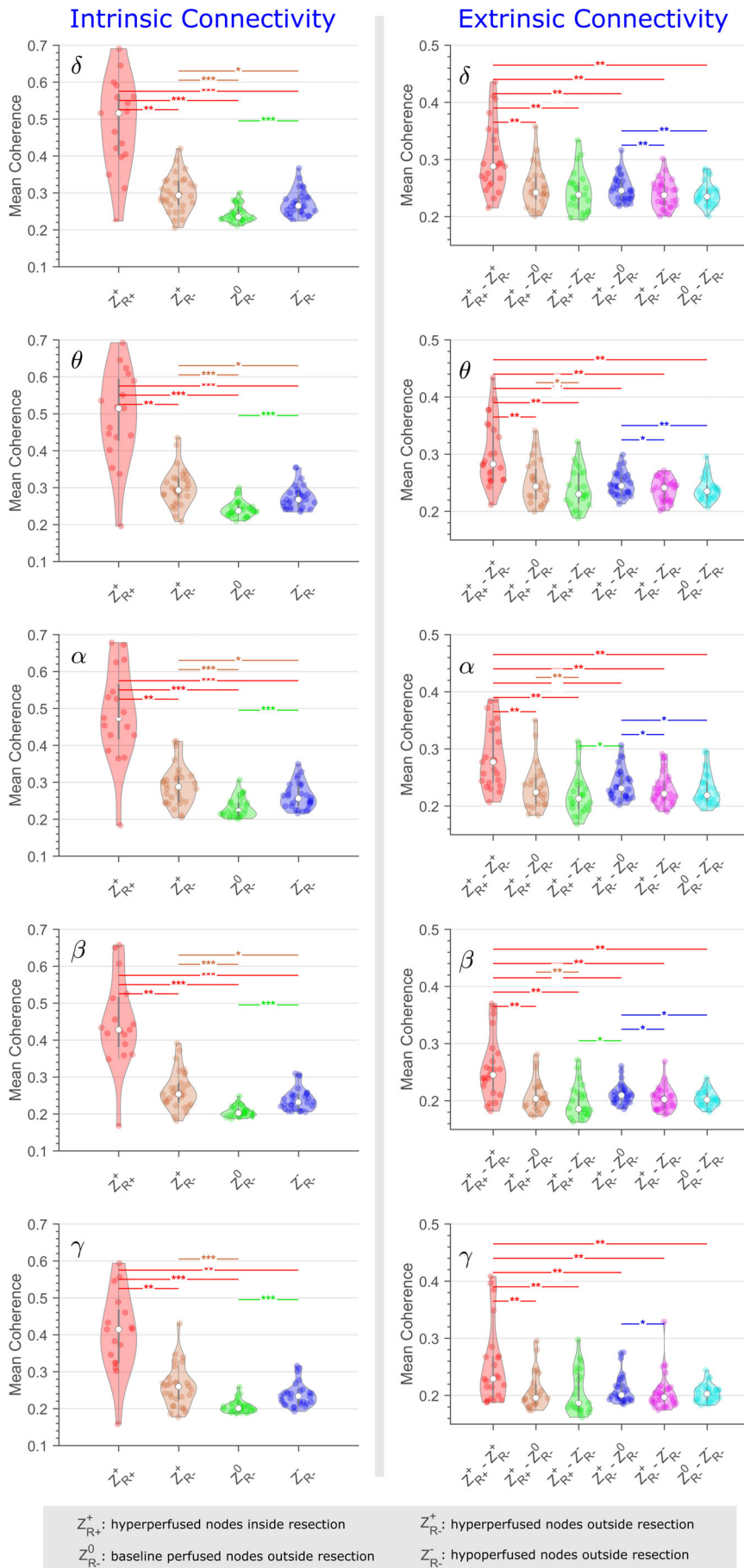
observed high correlation between β_1-coefficient and SISCOM z scores indicates that regions of ictal hyperperfusion have a positive β_1-coefficient, whereas regions of ictal hypoperfusion have a negative β_1-coefficient. The observed correlations were robust across methodologies used to estimate FC and frequencies of interest. Further, we report the presence of high intrinsic and extrinsic connectivity within and between hyperperfused brain regions inside and outside the area of surgical resection.

Congruent patterns of ictal hyperperfusion and semiological seizure progression have been described in temporal lobe epilepsy (Shin et al., 2002). The presence of electrophysiological and metabolic changes in areas of hyperperfusion at a distance from the EZ has been described using ictal scalp EEG (Kim et al., 2007), intracranial EEG (Spanaki et al., 1999), and PET studies (Bouilleret et al., 2002). Very few studies have investigated the resting-state FC within the nodes of seizure onset and seizure propagation. Our previous work has demonstrated first that electrical stimulation of the SEEG-defined seizure onset zone elicits a higher evoked response in the brain regions that showed hyperperfusion during preoperative ictal SPECT (Tousseyn et al., 2017), and second that SPECT perfusion patterns have strong electrophysiological underpinnings on intracranial EEG recordings (Krishnan et al., 2021). Blumenfeld et al. previously demonstrated that regions of reduced blood flow (hypoperfusion) during seizures exhibited increased power in the low-frequency bands on scalp EEG (Blumenfeld, McNally, et al., 2004; Krishnan et al., 2021).

We observed that high FC endures in the interictal state between brain regions that show hyperperfusion during seizures. Correspondence between interictal and ictal brain networks has been demonstrated by comparing the regions of SPECT hyperperfusion with interictal spike-related EEG-fMRI activation maps (Tousseyn et al., 2015). Studies have reported increased FC between regions implicated by interictal spikes—as compared to those unaffected by spikes (Bettus et al., 2011)—and the existence of preferential coupling within the EZ and between the EZ and propagation zone (Lagarde et al., 2018). Iasemidis et al. demonstrated that phase transition from the resting interictal state to the pathological ictal state occurs when critical brain regions are abnormally synchronized with each other (Iasemidis et al., 2003). These pathological synchronizations can occur minutes to hours before the seizure, while seizures occur to dynamically reset the pathological synchronization (Krishnan et al., 2011). Together, these results imply that ictally hyperperfused brain regions correspond to a strongly connected neuronal network during rest. Hence, the widespread and complex hyperperfusion patterns, which are often observed in ictal SPECT studies, are not random and represent functionally connected brain regions that are recruited in the course of the seizure.

Hypoperfusion
Compared to hyperperfusion, regions of hypoperfusion included a higher fraction of ROIs with statistically significant negative β_1-coefficients across patients and frequency bands. The negative β_1-coefficients imply that a strong interictal connection exists between regions of ictal hypoperfusion. Moreover, regions that

demonstrate ictal hypoperfusion have low interictal FC to regions that become hyperperfused during seizures. These findings are further supported by our intrinsic connectivity analysis, where we found that regions of ictal hypoperfusion have higher connectivity compared to baseline-perfused regions (areas that show no significant change in perfusion during seizures).

Studies have postulated that the ictal hypoperfusion of the frontoparietal association cortices observed in temporal lobe epilepsy (Van Paesschen et al., 2003) reflects a form of surround inhibition that seeks to limit the spread of seizures (Van Paesschen, 2004) or perhaps a functional deactivation of the frontoparietal cortices resulting from propagation of epileptiform activities to the upper brainstem reticular formation and the medial thalamus (Blumenfeld, McNally, et al., 2004). Moreover, intracranial EEG studies reveal ictal slowing in the frontal and parietal regions during temporal lobe seizures (Blumenfeld, Rivera, et al., 2004). Arthuis et al. noted a correlation of loss of consciousness during temporal lobe seizures with long-distance synchronization of electrophysiological signals in regions that are critical in the processing of awareness (including frontoparietal associative cortices and thalamus) (Arthuis et al., 2009). The existence of functional and structural connectivity between frontal and parietal cortices during rest is further supported by intracranial-EEG (Kucyi et al., 2018), fMRI (Lee et al., 2009), and DTI studies (Marshall et al., 2015). Regions of ictal hypoperfusion correspond to patterns of reduced blood oxygenation level-dependent (BOLD) signal observed in interictal spike-related EEG-fMRI studies in the same patients (Tousseyn et al., 2015). Such EEG-fMRI patterns of BOLD deactivation have been described within parts of the "default mode network" (comprising the posterior cingulate cortex, precuneus, medial frontal, and lateral parietal cortex) with both focal and generalized epileptic activities (Fahoum et al., 2013). Finally, electrical stimulation during SEEG recordings of the ictally hypoperfused brain regions (i.e., areas that showed ictal hypoperfusion in the preoperative SPECT study) elicited higher evoked responses in other hypoperfused (rather than hyperperfused) brain regions (Tousseyn et al., 2017). These results illustrate that brain regions, exhibiting hypoperfusion during seizures, belong to another distinct, interconnected neuronal network, which is separate from the hyperperfused seizure network. The discharging seizure focus recruits areas of seizure onset and spread (highlighted by ictal hyperperfusion). It also appears to modulate separate but interconnected brain regions, which become hypoperfused during the seizure without being directly connected to the patient's hyperperfused seizure network.

4.1.3 | Magnetoencephalography and epileptic network

Few studies have investigated epileptic networks using MEG. Malinowska et al. report similar spatiotemporal patterns when examining interictal spike discharges recorded using MEG and SEEG (Malinowska et al., 2014). Others have studied the spatio-temporal distribution of epileptiform discharges and high-frequency oscillations

to investigate the role of deep cortical and subcortical structures in seizure initiation and modulation utilizing multimodal analysis of EEG-fMRI or ictal MEG (Nissen et al., 2016; Rose et al., 2013; Vaudano et al., 2012).

Our study differs in that it directly investigates FC in the regions of ictal onset and propagation highlighted by ictal hyperperfusion. By combining information derived from dynamic seizure-related changes in perfusion with MEG FC, we can objectively investigate connectivity patterns that belong to patient-specific seizure networks. In addition, to advancing presurgical decision-making including the planning of intracranial electrode implantation and subsequent surgical intervention, we hope that this approach can contribute to our efforts to modulate pathological epileptic networks and develop patient-specific therapeutic interventions.

4.1.4 | Intrinsic and extrinsic connectivity within the epileptic network

Our study shows that ictally hyperperfused ROIs residing both inside and outside the resected cortex have higher intrinsic FC when compared to baseline perfused areas (where perfusion does not change during the seizure), and ictally hypoperfused ROIs that reside outside the resected cortex. Across patients, we observed a gradient in intrinsic connectivity, with the highest connectivity values residing within the resected areas of hyperperfusion, followed in descending order by areas of ictal hyperperfusion, hypoperfusion, and lastly baseline perfusion that had not been included in the surgical resection. Further, we observed higher extrinsic connectivity between regions of hyperperfusion that resided within the resective cavity, as compared to those outside the area of resection. The average intrinsic and extrinsic connectivity were independent of the prognosis following surgery, the timing of ictal SPECT injection, and the duration of the seizure. Results from this study corroborate our previous findings and highlight the fact that the ictally hyperperfused brain regions correspond to a strongly connected brain network during rest irrespective of surgical outcomes (Tousseyn et al., 2017). Similarly, SEEG studies examining intrinsic FC in the interictal state have shown higher FC within the EZ, within the seizure propagation zone, and between the epileptogenic and propagation zones (Lagarde et al., 2018).

For coherence-based FC analysis, we observed a statistically significant, higher, intrinsic connectivity within hyperperfused brain regions residing inside the resective cavity, as compared to the ones outside the area of resection. These differences were significant only for patients who were seizure-free following resective epilepsy surgery. Hence, coherence-based connectivity analysis could be used to noninvasively identify and target critical nodes of hyperperfusion. A less favorable seizure outcome would be more likely when critical parts of the hyperperfusion network have been omitted from the final surgical resection. MEG and EEG studies of interictal FC have demonstrated elevated synchrony within the EZ (Englot et al., 2015; Krishnan et al., 2015; Lagarde et al., 2018; Vlachos et al., 2016) and have linked positive surgical outcomes with resection of regions that

exhibit high local synchrony (Antony et al., 2013). Coherence analysis of ictal SEEG discharges has demonstrated synchronized intracranial EEG patterns with the areas of seizure onset and seizure propagation (Bartolomei et al., 1999). Epileptogenic processes mediate neuronal network reconfiguration resulting in abnormal connectivity within the EZ (Blumenfeld et al., 2007; Percha et al., 2005). Our study illustrates that FC within the EZ is indeed elevated even during resting-state conditions.

Lastly, we observed a higher but not statistically significant connectivity value in areas of ictal hyperperfusion that resided within the resective cavity (as compared to areas of hyperperfusion that were not included in the resection), when employing PLV as the FC estimator. PLV is a nonlinear measure of connectivity, sensitive to phase consistencies between signals, whereas coherence is sensitive to phase and amplitude consistencies of signals. The divergent sensitivities of the two measures to different aspects of the signal could explain the differences in our results.

Our prior investigations comparing SPECT perfusion patterns with intracranial EEG activity during semiologically identical seizures in the same patient have shown that power spectral changes in alpha to high-frequency bands were higher in areas that showed hyperperfusion, as compared to areas that exhibited baseline (unchanged perfusion) or hypoperfusion during the ictal SPECT seizure (Krishnan et al., 2021). The lack of significant frequency-specific connectivity relations in the current study could be attributable to differences in methodology (power spectral analysis vs. FC), and discrepancies in brain states (ictal vs. resting state).

4.2 | Clinical implication

Invasive surgical planning using stereo-EEG relies on a priori identification of the critical brain regions that constitute the epileptic network using seizure semiology, electroclinical correlations, and a plethora of noninvasive diagnostic modalities. This noninvasive, a priori, definition of the critical epileptogenic network is not a trivial problem. The proposed, combined analysis of SPECT perfusion patterns during seizures along with resting-state (interictal) MEG FC provides us with an objective criterion for the a priori identification of critical regions that are influenced by a patient-specific epileptogenic process.

Importantly, this novel noninvasive approach can also aid in the a posteriori interpretation of complex, sparse or inconclusive, SEEG recordings. Prospective validation in a large dataset is a mandatory next step. Nonetheless, our results would predict a favorable seizure outcome when the planned surgical resection incorporates nodes of ictal hyperperfusion with significantly higher intrinsic MEG connectivity, as opposed to other areas of hyperperfusion.

Our study indicates that connectivity within the ictally hyperperfused network is increased not only during seizures but also during the interictal state. These same interictal networks could facilitate the neuromodulatory effects of chronic neurostimulation—such as direct cortical or deep brain stimulation—where electrical impulses are

delivered interictally (Yu et al., 2018) to moderate network dynamics and thus suppress the occurrence of epileptic seizures (Shon et al., 2005; Van Laere et al., 2002). The results of this study have important clinical implications insofar as they introduce a measurable noninvasive framework that could be exploited to select, tailor, or adjust therapeutic interventions based on patient-specific epileptic networks.

4.3 | Methodological constraints and limitations

4.3.1 | Subtraction ictal SPECT

SPECT hyperperfusion patterns provide a snapshot of the regions associated with ictal onset and propagation. The fast dynamics associated with an ictal event complicate the interpretation of the static SPECT perfusion patterns. Specific statistical thresholds determined by clinical considerations are used to aid the interpretation of SPECT studies. Our definition of hyper- and hypo-perfused brain regions was motivated by the findings of Newey et al., who showed that a SISCOM z scores of 1.5 have the highest sensitivity and specificity in localizing the EZ (Newey et al., 2013). However, the defined threshold may be suboptimal in delineating the epileptic network. With this limitation in mind, we performed a two-fold analysis by considering the entire spectrum of SISCOM z scores, while also looking at thresholded SISCOM z-maps. The results were similar irrespective of the analysis, that is, two discrete but strongly connected networks can be identified in the interictal state, when informed by the patterns of significant hyperperfusion, and separately significant hypoperfusion, during seizures. The localization value of SPECT studies is considered to be higher with an early ictal injection of the radiotracer (Lee et al., 2011), and with injection during focal seizures that do not evolve to secondary generalization (Varghese et al., 2009). It is important to note that the observed correlations between SPECT and FC were quite robust and were not significantly impacted by early vs. late timing of ictal SPECT injection, secondary generalization versus nongeneralized SPECT seizure, presence of one (uni-focal) versus more than one (multi-focal) SEEG onset regions, and seizure-free versus nonseizure-free outcome. This could be explained by the fact that our study intended to investigate connectivity at a larger scale and was not focused solely on localizing the EZ.

4.3.2 | Functional connectivity analysis

Source level FC analysis using MEG relies on inverse modeling of sensor time series. This approach is ill-posed and can lead to nonunique solutions. Different mathematical approaches exist for the inverse modeling of MEG sensor data. In our study, we selected dSPM for inverse modeling, since it is considered to be more sensitive to deeper sources (Dale et al., 2000).

While MEG is not impeded by the thickness and integrity of the skull and dura, the sensitivity of MEG to detect brain activity drops off as the square of the distance from the sensor. Hence, MEG has difficulty recording activity from deeper brain regions, especially from subcortical structures—although recent studies have suggested that MEG could potentially detect brain activity arising from such deep sources (Pizzo et al., 2019).

The state of the brain such as sleep, wakefulness, and so on affects FC estimates (Tagliazucchi & Laufs, 2014; Turner et al., 2020; Usami et al., 2015). The retrospective nature of our study limits our ability to control the patient's brain state. The MEG study was performed to record interictal epileptiform discharges. The yield of interictal discharges increases when the subject is in a state of sleep. Hence, a majority of the patients in this study were asleep during the MEG recording session. We found increased connectivity in the alpha frequency band within the hypoperfused regions in patients who were in a state of wakefulness, as compared to patients who were asleep during the MEG. The reduced connectivity in the alpha frequency band during sleep likely results from the attenuation of alpha waves during sleep. Our study was ill-powered to assess the difference in resting-state connectivity between different sleep stages. Hence, the results of this study should be interpreted in light of these limitations taking into account the constraints inherent to retrospective studies.

Functional connectivity can be defined as a descriptive measure of spatiotemporal correlations that exist between spatially distinct regions of the brain (Friston et al., 1993). PLV and coherence are two commonly employed nondirectional measures used to quantify phase synchrony between neuronal signals. We observed that the PLV-based connectivity estimator was more robust in elucidating SPECT-connectivity correlations across patients—when compared to coherence analysis. Deviation of spectral coherence measures from ideal estimates can occur in a high noise environment, and when oscillators exhibit intermittent synchronization (Lowet et al., 2016). We should note that neuronal oscillations can produce intermittent synchronizations and can affect cortical synchrony estimation using coherence. PLV has better noise properties and is less influenced by the nonstationarity of neuronal signals, whereas coherence-based analysis is more sensitive to amplitude relationships between signals.

5 | CONCLUSION

Our multimodal study combining ictal SPECT with resting-state MEG connectivity analysis demonstrates that the widespread patterns of areas of hyperperfusion, as well as hypoperfusion, during seizures are not at all arbitrary. Rather they highlight nonrandom brain regions that remain interconnected during the interictal state. The combination of SPECT and MEG can provide a measurable, noninvasive, definition of patient-specific epileptic networks. In addition to advancing surgical decisions including strategy for implantation of invasive electrodes or neurostimulators, we hope that this approach will contribute to our efforts to understand and modulate pathological epileptic networks and establish individualized, patient-specific diagnostic and therapeutic interventions.

CONFLICT OF INTEREST

None of the authors has any conflict of interest to disclose. We confirm that we have read the Journal's position on issues involved in ethical publication and affirm that this report is consistent with those guidelines.

DATA AVAILABILITY STATEMENT

Raw MEG and SPECT data are not publicly available due to patient privacy restrictions. However, de-identified data can be made available upon reasonable request and completion of a formal data-sharing agreement.

ORCID

Balu Krishnan https://orcid.org/0000-0002-1897-3359

REFERENCES

Antony, A. R., Alexopoulos, A. V., González-Martínez, J. A., Mosher, J. C., Jehi, L., Burgess, R. C., So, N. K., & Galán, R. F. (2013). Functional connectivity estimated from intracranial EEG predicts surgical outcome in intractable temporal lobe epilepsy. *PLoS One*, *8*, e77916. https://doi.org/10.1371/journal.pone.0077916

Arthuis, M., Valton, L., Régis, J., Chauvel, P., Wendling, F., Naccache, L., Bernard, C., & Bartolomei, F. (2009). Impaired consciousness during temporal lobe seizures is related to increased long-distance cortical–subcortical synchronization. *Brain*, *132*, 2091–2101. https://doi.org/10.1093/brain/awp086

Bartolomei, F., Wendling, F., Vignal, J.-P., Kochen, S., Bellanger, J.-J., Badier, J.-M., Le Bouquin-Jeannes, R., & Chauvel, P. (1999). Seizures of temporal lobe epilepsy: Identification of subtypes by coherence analysis using stereo-electro-encephalography. *Clinical Neurophysiology*, *110*, 1741–1754. https://doi.org/10.1016/S1388-2457(99)00107-8

Benjamini, Y., & Hochberg, Y. (1995). Controlling the false discovery rate: A practical and powerful approach to multiple testing. *Journal of the Royal Statistical Society, Series B*, *57*, 289–300. https://doi.org/10.2307/2346101

Bettus, G., Ranjeva, J.-P., Wendling, F., Bénar, C. G., Confort-Gouny, S., Régis, J., Chauvel, P., Cozzone, P. J., Lemieux, L., Bartolomei, F., & Guye, M. (2011). Interictal functional connectivity of human epileptic networks assessed by intracerebral EEG and BOLD signal fluctuations. *PLoS One*, *6*, e20071. https://doi.org/10.1371/journal.pone.0020071

Blumenfeld, H., McNally, K. A., Vanderhill, S. D., Paige, A. L., Chung, R., Davis, K., Norden, A. D., Stokking, R., Studholme, C., Novotny, E. J., Zubal, I. G., & Spencer, S. S. (2004). Positive and negative network correlations in temporal lobe epilepsy. *Cerebral Cortex*, *14*, 892–902. https://doi.org/10.1093/cercor/bhh048

Blumenfeld, H., Rivera, M., McNally, K. A., Davis, K., Spencer, D. D., & Spencer, S. S. (2004). Ictal neocortical slowing in temporal lobe epilepsy. *Neurology*, *63*, 1015–1021. https://doi.org/10.1212/01.WNL.0000141086.91077.CD

Blumenfeld, H., Rivera, M., Vasquez, J. G., Shah, A., Ismail, D., Enev, M., & Zaveri, H. P. (2007). Neocortical and thalamic spread of amygdala kindled seizures. *Epilepsia*, *48*, 254–262. https://doi.org/10.1111/j.1528-1167.2006.00934.x

Bokil, H., Andrews, P., Kulkarni, J. E., Mehta, S., & Mitra, P. P. (2010). Chronux: A platform for analyzing neural signals. *Journal of Neuroscience Methods*, *192*, 146–151. https://doi.org/10.1016/J.JNEUMETH.2010.06.020

Bouilleret, V., Valenti, M. P., Hirsch, E., Semah, F., & Namer, I. J. (2002). Correlation between PET and SISCOM in temporal lobe epilepsy. *Journal of Nuclear Medicine*, *43*, 991–998.

Cleeren, E., Premereur, E., Casteels, C., Goffin, K., Janssen, P., & Van Paesschen, W. (2016). The effective connectivity of the seizure onset zone and ictal perfusion changes in amygdala kindled rhesus monkeys. *NeuroImage: Clinical*, *12*, 252–261. https://doi.org/10.1016/j.nicl.2016.05.020

Dale, A. M., Fischl, B., & Sereno, M. I. (1999). Cortical surface-based analysis: I. Segmentation and surface reconstruction. *NeuroImage*, *9*, 179–194. https://doi.org/10.1006/nimg.1998.0395

Dale, A. M., Liu, A. K., Fischl, B. R., Buckner, R. L., Belliveau, J. W., Lewine, J. D., & Halgren, E. (2000). Dynamic statistical parametric mapping: Combining fMRI and MEG for high-resolution imaging of cortical activity. *Neuron*, *26*, 55–67.

Dupont, P., Van Paesschen, W., Palmini, A., Ambayi, R., Van Loon, J., Goffin, J., Weckhuysen, S., Sunaert, S., Thomas, B., Demaerel, P., Sciot, R., Becker, A. J., Vanbilloen, H., Mortelmans, L., & Van Laere, K. (2006). Ictal perfusion patterns associated with single MRI-visible focal dysplastic lesions: Implications for the noninvasive delineation of the epileptogenic zone. *Epilepsia*, *47*, 1550–1557. https://doi.org/10.1111/j.1528-1167.2006.00628.x

El Tahry, R., Wang, Z. I., Thandar, A., Podkorytova, I., Krishnan, B., Tousseyn, S., Guiyun, W., Burgess, R. C., & Alexopoulos, A. V. (2018). Magnetoencephalography and ictal SPECT in patients with failed epilepsy surgery. *Clinical Neurophysiology*, *129*, 1651–1657. https://doi.org/10.1016/J.CLINPH.2018.05.010

Englot, D. J., Hinkley, L. B., Kort, N. S., Imber, B. S., Mizuiri, D., Honma, S. M., Findlay, A. M., Garrett, C., Cheung, P. L., Mantle, M., Tarapore, P. E., Knowlton, R. C., Chang, E. F., Kirsch, H. E., & Nagarajan, S. S. (2015). Global and regional functional connectivity maps of neural oscillations in focal epilepsy. *Brain*, *138*, 2249–2262. https://doi.org/10.1093/brain/awv130

Englot, D. J., & Lagrange, A. H. (2022). Of blobs and buzzes: Does SISCOM imaging actually help SEEG planning? *Epilepsy Currents*, *22*(1), 22–24. https://doi.org/10.1177/15357597211025408

Fahoum, F., Zelmann, R., Tyvaert, L., Dubeau, F., & Gotman, J. (2013). Epileptic discharges affect the default mode network – fMRI and intracerebral EEG evidence. *PLoS One*, *8*, e68038. https://doi.org/10.1371/journal.pone.0068038

Friston, K. J., Frith, C. D., Liddle, P. F., & Frackowiak, R. S. J. (1993). Functional connectivity: The principal-component analysis of large (PET) data sets. *Journal of Cerebral Blood Flow & Metabolism*, 13, 5–14. https://doi.org/10.1038/jcbfm.1993.4

Halász, P. (2010). The concept of epileptic networks. Part 1. *Ideggyógyászati Szemle*, 63, 293–303.

Honey, C. J., Sporns, O., Cammoun, L., Gigandet, X., Thiran, J. P., Meuli, R., & Hagmann, P. (2009). Predicting human resting-state functional connectivity from structural connectivity. *Proceedings of the National Academy of Sciences*, 106, 2035–2040. https://doi.org/10.1073/pnas.0811168106

Huang, M. X., Mosher, J. C., & Leahy, R. M. (1999). A sensor-weighted overlapping-sphere head model and exhaustive head model comparison for MEG. *Physics in Medicine and Biology*, 44, 423–440.

Hyvärinen, A., & Oja, E. (2000). Independent component analysis: Algorithms and applications. *Neural Networks*, 13, 411–430. https://doi.org/10.1016/S0893-6080(00)00026-5

Iasemidis, L. D., Pardalos, P. M., Shiau, D. S., Chaovalitwongse, W., Narayanan, K., Kumar, S., Carney, P. R., & Sackellares, J. C. (2003). Prediction of human epileptic seizures based on optimization and phase changes of brain electrical activity. *Optimization Methods and Software*, 18, 81–104.

Kakisaka, Y., Wang, Z. I., Mosher, J. C., Dubarry, A.-S., Alexopoulos, A. V., Enatsu, R., Kotagal, P., & Burgess, R. C. (2012). Clinical evidence for the utility of movement compensation algorithm in magnetoencephalography: Successful localization during focal seizure. *Epilepsy Research*, 101, 191–196.

Kaminska, A., Chiron, C., Ville, D., Dellatolas, G., Hollo, A., Cieuta, C., Jalin, C., Delalande, O., Fohlen, M., Vera, P., Soufflet, C., & Dulac, O. (2003). Ictal SPECT in children with epilepsy: Comparison with intracranial EEG and relation to postsurgical outcome. *Brain*, 126, 248–260. https://doi.org/10.1093/brain/awg013

Kim, J. H., Im, K. C., Kim, J. S., Lee, S.-A., Lee, J. K., Khang, S. K., & Kang, J. K. (2007). Ictal hyperperfusion patterns in relation to ictal scalp EEG patterns in patients with unilateral hippocampal sclerosis: A SPECT study. *Epilepsia*, 48, 270–277. https://doi.org/10.1111/j.1528-1167.2006.00847.x

Knowlton, R. C., Elgavish, R. A., Limdi, N., Bartolucci, A., Ojha, B., Blount, J., Burneo, J. G., Ver Hoef, L., Paige, L., Faught, E., Kankirawatana, P., Riley, K., & Kuzniecky, R. (2008). Functional imaging: I. relative predictive value of intracranial electroencephalography. *Annals of Neurology*, 64, 25–34. https://doi.org/10.1002/ana.21389

Kramer, M. A., & Cash, S. S. (2012). Epilepsy as a disorder of cortical network organization. *The Neuroscientist*, 18, 360–372. https://doi.org/10.1177/1073858411422754

Krishnan, B., Faith, A., Vlachos, I., Roth, A., Williams, K., Noe, K., Drazkowski, J., Tapsell, L., Sirven, J., & Iasemidis, L. (2011). Resetting of brain dynamics: Epileptic versus psychogenic nonepileptic seizures. *Epilepsy & Behavior*, 22, S74–S81.

Krishnan, B., Tousseyn, S., Sateesh Nayak, C., Aung, T., Kheder, A., Wang, Z. I., Wu, G., Gonzalez-Martinez, J., Nair, D., Burgess, R., Iasemidis, L., Najm, I., Bulacio, J., & Alexopoulos, A. V. (2021). Neurovascular networks in epilepsy: Correlating ictal blood perfusion with intracranial electrophysiology. *NeuroImage*, 231, 117838.

Krishnan, B., Vlachos, I., Wang, Z. I., Mosher, J., Najm, I., Burgess, R., Iasemidis, L., & Alexopoulos, A. V. (2015). Epileptic focus localization based on resting state interictal MEG recordings is feasible irrespective of the presence or absence of spikes. *Clinical Neurophysiology*, 126, 667–674. https://doi.org/10.1016/j.clinph.2014.07.014

Kucyi, A., Schrouff, J., Bickel, S., Foster, B. L., Shine, J. M., & Parvizi, J. (2018). Intracranial electrophysiology reveals reproducible intrinsic functional connectivity within human brain networks. *The Journal of Neuroscience*, 38, 4230–4242. https://doi.org/10.1523/JNEUROSCI.0217-18.2018

Lachaux, J. P., Rodriguez, E., Martinerie, J., & Varela, F. J. (1999). Measuring phase synchrony in brain signals. *Human Brain Mapping*, 8, 194–208.

Lagarde, S., Roehri, N., Lambert, I., Trebuchon, A., McGonigal, A., Carron, R., Scavarda, D., Milh, M., Pizzo, F., Colombet, B., Giusiano, B., Medina Villalon, S., Guye, M., Bénar, C.-G., & Bartolomei, F. (2018). Interictal stereotactic-EEG functional connectivity in refractory focal epilepsies. *Brain*, 141, 2966–2980. https://doi.org/10.1093/brain/awy214

Lee, J. Y., Joo, E. Y., Park, H. S., Song, P., Young Byun, S., Seo, D. W., & Hong, S. B. (2011). Repeated ictal SPECT in partial epilepsy patients: SISCOM analysis. *Epilepsia*, 52, 2249–2256. https://doi.org/10.1111/j.1528-1167.2011.03257.x

Lee, U., Kim, S., Noh, G.-J., Choi, B.-M., Hwang, E., & Mashour, G. A. (2009). The directionality and functional organization of frontoparietal connectivity during consciousness and anesthesia in humans. *Consciousness and Cognition*, 18, 1069–1078. https://doi.org/10.1016/J.CONCOG.2009.04.004

Lowet, E., Roberts, M. J., Bonizzi, P., Karel, J., & De Weerd, P. (2016). Quantifying neural oscillatory synchronization: A comparison between spectral coherence and phase-locking value approaches. *PLoS One*, 11, e0146443. https://doi.org/10.1371/journal.pone.0146443

Malinowska, U., Badier, J. M., Gavaret, M., Bartolomei, F., Chauvel, P., & Bénar, C. G. (2014). Interictal networks in magnetoencephalography. *Human Brain Mapping*, 35, 2789–2805. https://doi.org/10.1002/hbm.22367

Marshall, T. R., Bergmann, T. O., & Jensen, O. (2015). Frontoparietal structural connectivity mediates the top-down control of neuronal synchronization associated with selective attention. *PLoS Biology*, 13, e1002272. https://doi.org/10.1371/journal.pbio.1002272

Murakami, H., Wang, Z. I., Marashly, A., Krishnan, B., Prayson, R. A., Kakisaka, Y., Mosher, J. C., Bulacio, J., Gonzalez-Martinez, J. A., Bingaman, W. E., Najm, I. M., Burgess, R. C., & Alexopoulos, A. V. (2016). Correlating magnetoencephalography to stereo-electroencephalography in patients undergoing epilepsy surgery. *Brain*, 139, 2935–2947. https://doi.org/10.1093/brain/aww215

Newey, C. R., Wong, C., Irene Wang, Z., Chen, X., Wu, G., & Alexopoulos, A. V. (2013). Optimizing SPECT SISCOM analysis to localize seizure-onset zone by using varying z scores. *Epilepsia*, 54, 793–800. https://doi.org/10.1111/epi.12139

Newton, M. R., Berkovic, S. F., Austin, M. C., Rowe, C. C., McKay, W. J., & Bladin, P. F. (1995). SPECT in the localisation of extratemporal and temporal seizure foci. *Journal of Neurology, Neurosurgery, and Psychiatry*, 59, 26–30. https://doi.org/10.1136/JNNP.59.1.26

Nissen, I. A., van Klink, N. E. C., Zijlmans, M., Stam, C. J., & Hillebrand, A. (2016). Brain areas with epileptic high frequency oscillations are functionally isolated in MEG virtual electrode networks. *Clinical Neurophysiology*, 127, 2581–2591. https://doi.org/10.1016/J.CLINPH.2016.04.013

Percha, B., Dzakpasu, R., Zochowski, M., & Parent, J. (2005). Transition from local to global phase synchrony in small world neural network and its possible implications for epilepsy. *Physical Review E: Statistical, Nonlinear, and Soft Matter Physics*, 72, 031909. https://doi.org/10.1103/PhysRevE.72.031909

Pizzo, F., Roehri, N., Medina Villalon, S., Trébuchon, A., Chen, S., Lagarde, S., Carron, R., Gavaret, M., Giusiano, B., McGonigal, A., Bartolomei, F., Badier, J. M., & Bénar, C. G. (2019). Deep brain activities can be detected with magnetoencephalography. *Nature Communications*, 10, 971. https://doi.org/10.1038/s41467-019-08665-5

Rose, D. F., Fujiwara, H., Holland-Bouley, K., Greiner, H. M., Arthur, T., & Mangano, F. T. (2013). Focal peak activities in spread of interictal-ictal discharges in epilepsy with beamformer MEG: Evidence for an epileptic network? *Frontiers in Neurology*, 4, 56. https://doi.org/10.3389/fneur.2013.00056

Schneider, F., Irene Wang, Z., Alexopoulos, A. V., Almubarak, S., Kakisaka, Y., Jin, K., Nair, D., Mosher, J. C., Najm, I. M., & Burgess, R. C. (2013). Magnetic source imaging and ictal SPECT in MRI-negative neocortical epilepsies: Additional value and comparison with intracranial EEG. *Epilepsia*, *54*, 359–369. https://doi.org/10.1111/epi.12004

Shin, W. C., Hong, S. B., Tae, W. S., & Kim, S. E. (2002). Ictal hyperperfusion patterns according to the progression of temporal lobe seizures. *Neurology*, *58*, 373–380. https://doi.org/10.1212/WNL.58.3.373

Shon, Y.-M., Lee, K. J., Kim, H. J., Chung, Y.-A., Ahn, K. J., Kim, Y. I., Yang, D. W., & Kim, B. S. (2005). Effect of chronic deep brain stimulation of the subthalamic nucleus for frontal lobe epilepsy: Subtraction SPECT analysis. *Stereotactic and Functional Neurosurgery*, *83*, 84–90. https://doi.org/10.1159/000086867

Spanaki, M. V., Zubal, I. G., MacMullan, J., & Spencer, S. S. (1999). Periictal SPECT localization verified by simultaneous intracranial EEG. *Epilepsia*, *40*, 267–274. https://doi.org/10.1111/j.1528-1157.1999.tb00703.x

Spencer, S. S. (2002). Neural networks in human epilepsy: Evidence of and implications for treatment. *Epilepsia*, *43*, 219–227.

Tadel, F., Baillet, S., Mosher, J. C., Pantazis, D., & Leahy, R. M. (2011). Brainstorm: A user-friendly application for MEG/EEG analysis. *Computational Intelligence and Neuroscience*, *2011*, 879716. https://doi.org/10.1155/2011/879716

Tagliazucchi, E., & Laufs, H. (2014). Decoding wakefulness levels from typical fMRI resting-state data reveals reliable drifts between wakefulness and sleep. *Neuron*, *82*, 695–708. https://doi.org/10.1016/J.NEURON.2014.03.020

Taulu, S., & Hari, R. (2009). Removal of magnetoencephalographic artifacts with temporal signal-space separation: Demonstration with single-trial auditory-evoked responses. *Human Brain Mapping*, *30*, 1524–1534. https://doi.org/10.1002/hbm.20627

Thomson, D. J. (1982). Spectrum estimation and harmonic analysis. *Proceedings of the IEEE*, *70*, 1055–1096. https://doi.org/10.1109/PROC.1982.12433

Tousseyn, S., Dupont, P., Goffin, K., Sunaert, S., & Van Paesschen, W. (2015). Correspondence between large-scale ictal and interictal epileptic networks revealed by single photon emission computed tomography (SPECT) and electroencephalography (EEG)-functional magnetic resonance imaging (fMRI). *Epilepsia*, *56*, 382–392. https://doi.org/10.1111/epi.12910

Tousseyn, S., Krishnan, B., Wang, Z. I., Wongwiangjunt, S., Nayak, C. S., Mosher, J. C., Wu, G., Van Paesschen, W., Leahy, R. M., Gonzalez-Martinez, J. A., Bulacio, J., Najm, I. M., Alexopoulos, A. V., & Nair, D. R. (2017). Connectivity in ictal single photon emission computed tomography perfusion: A cortico-cortical evoked potential study. *Brain*, *42*, 282–286. https://doi.org/10.1093/brain/awx123

Turner, K. L., Gheres, K. W., Proctor, E. A., & Drew, P. J. (2020). Neurovascular coupling and bilateral connectivity during NREM and REM sleep. *eLife*, *9*, 1. https://doi.org/10.7554/ELIFE.62071

Usami, K., Matsumoto, R., Kobayashi, K., Hitomi, T., Shimotake, A., Kikuchi, T., Matsuhashi, M., Kunieda, T., Mikuni, N., Miyamoto, S., Fukuyama, H., Takahashi, R., & Ikeda, A. (2015). Sleep modulates

cortical connectivity and excitability in humans: Direct evidence from neural activity induced by single-pulse electrical stimulation. *Human Brain Mapping*, *36*, 4714–4729. https://doi.org/10.1002/HBM.22948

Van Laere, K., Vonck, K., Boon, P., Versijpt, J., & Dierckx, R. (2002). Perfusion SPECT changes after acute and chronic vagus nerve stimulation in relation to prestimulus condition and long-term clinical efficacy. *Journal of Nuclear Medicine*, *43*, 733 LP–744.

Van Paesschen, W. (2004). Ictal SPECT. *Epilepsia*, *45*, 35–40. https://doi.org/10.1111/j.0013-9580.2004.04008.x

Van Paesschen, W., Dupont, P., Van Driel, G., Van Billoen, H., & Maes, A. (2003). SPECT perfusion changes during complex partial seizures in patients with hippocampal sclerosis. *Brain*, *126*, 1103–1111. https://doi.org/10.1093/brain/awg108

Varghese, G. I., Purcaro, M. J., Motelow, J. E., Enev, M., McNally, K. A., Levin, A. R., Hirsch, L. J., Tikofsky, R., Paige, A. L., Zubal, I. G., Spencer, S. S., & Blumenfeld, H. (2009). Clinical use of ictal SPECT in secondarily generalized tonic–clonic seizures. *Brain*, *132*, 2102–2113. https://doi.org/10.1093/brain/awp027

Vaudano, A. E., Carmichael, D. W., Salek-Haddadi, A., Rampp, S., Stefan, H., Lemieux, L., & Koepp, M. J. (2012). Networks involved in seizure initiation. A reading epilepsy case studied with EEG-fMRI and MEG. *Neurology*, *79*, 249–253. https://doi.org/10.1212/WNL.0b013e31825fdf3a

Vlachos, I., Krishnan, B., Treiman, D., Tsakalis, K., Kugiumtzis, D., & Iasemidis, L. (2016). The concept of effective inflow: Application to interictal localization of the epileptogenic focus from iEEG. *IEEE Transactions on Bio-medical Engineering*, *64*, 2241–2252. https://doi.org/10.1109/TBME.2016.2633200

Yu, T., Wang, X., Li, Y., Zhang, G., Worrell, G., Chauvel, P., Ni, D., Qiao, L., Liu, C., Li, L., Ren, L., & Wang, Y. (2018). High-frequency stimulation of anterior nucleus of thalamus desynchronizes epileptic network in humans. *Brain*, *141*, 2631–2643. https://doi.org/10.1093/BRAIN/AWY187

SUPPORTING INFORMATION

Additional supporting information can be found online in the Supporting Information section at the end of this article.